Journal of
Ceramic Science
and Technology

J. Ceram. Sci. Technol., **12** [2] 115-124 (2021)
DOI: 10.4416/JCST2021-00012
available online at: http://www.ceramic-science.com

Effect of ZrO_2 Doping on Strength and Toughness of Mo_2NiB_2-Based Cermets

W. Li*, Z. Fan, T. Ai, H. Dong, P. Jiang, X. Zou

Shaanxi University of Technology, Dongyihuan Road, Hanzhong City, 723000, Shaanxi province, China
received July 12, 2021; received in revised form October 4, 2021; accepted October 11, 2021

Abstract

Mo_2NiB_2-based cermets possess superior strength and excellent corrosion resistance, however, they usually exhibit poor toughness at room temperature. An improvement in toughness without reducing their strength is critical for the practical application of cermets. In this study, four series of Mo_2NiB_2-based cermets doped with ZrO_2 particles (0 wt%, 1.0 wt%, 1.5 wt% and 2.0 wt%) were fabricated based on the boronizing sintering reaction of a mixture of ball-milled Mo-Ni-B-ZrO_2 powders. The effect of the ZrO_2 content on the microstructure and crystalline phases was investigated by means of transmission electron microscopy (TEM), scanning electron microscopy (SEM), energy dispersive X-ray analysis (EDX), electron back-scattered diffraction (EBSD) and X-ray diffraction (XRD). The flexural strength and fracture toughness of the developed materials were also evaluated. At a ZrO_2 mass fraction of 1.0 wt%, the sintered cermet exhibited an optimal microstructure consisting of a continuous Ni phase with embedded Mo_2NiB_2 (~ 0.5 µm) particles. The Mo_2NiB_2-based cermet doped with 1.0 wt% ZrO_2 particles displayed the highest flexural strength (1 397.33 MPa), along with significantly enhanced fracture toughness (24.08 MPa $m^{1/2}$). The enhanced strength could be attributed to the increased dislocation density as well as the obstruction to grain boundary slip caused by the ZrO_2 particles. Further, the improved toughness might be attributed to crack deflection, crack bridging, transgranular cracks and ZrO_2 phase transformation. This study provides the experimental and theoretical basis for the development of the Mo_2NiB_2-based cermets.

Keywords: Mo_2NiB_2-based cermets, flexural strength, fracture toughness, strengthening and toughening mechanism

I. Introduction

Among the Mo-Ni-B systems, the two-phase cermets consisting of the Ni-bonded and Mo_2NiB_2 phases exhibit attractive potential for structural application at elevated temperatures [1,2]. The Mo_2NiB_2 phase demonstrates excellent creep and compression strength as well as high hardness (> 84.5 HRA) and flexural strength (~ 1 700 MPa) [3]. However, these intermetallic compounds suffer from very low fracture toughness at room temperature. To improve their fracture toughness and bending strength, an alloying technology or a composites approach is required, as also pursued by Takagi [4]. It was observed that the crystal structure of Mo_2NiB_2 ternary boride changed from orthorhombic to tetragonal on incorporating Cr and V [3,5], however, the addition of other alloying elements (such as Fe, Co, Ti, Mn, Zr, Nb and W) did not induce any structural change and strengthening [6,7]. The structural transformation is beneficial for improving the mechanical properties of the ternary boride cermet owing to the high degree of isotropy of the tetragonal boride phase, fine grain size of the tetragonal boride phase and superior microstructural homogeneity. However, the changes in the crystal structure of Mo_2NiB_2 ternary boride have an insignificant effect on the toughness.

Numerous studies have reported that the incorporation of oxide, boride or carbide in cermets can hinder the growth of the grain boundaries and refine the grain size [8–10]. R. Li *et al.* demonstrated that for a multiphase Mo-Si-B system, the spherical or ellipsoidal ZrO_2/Mo_2Zr particles at the nano- and submicron scales were located at the grain boundaries and partially in the grain interior, which proved that the Zr addition was beneficial for improving the fracture toughness of the Mo-12Si-8.5B alloy [11]. Additionally, J. Wang *et al.* pointed out that the compressive strength increased to 3.13 GPa when ZrB was incorporated. Further, the fracture toughness increased by about 27 % and reached a value of 11.5 MPa $m^{1/2}$ at 1.0 wt% ZrB_2 [12]. Moreover, C. Hochmuth *et al.* reported that the ZrO_2 phases were distributed at the grain boundaries and within the grains, which improved the creep properties of the Mo-Si-B alloy [13].

ZrO_2 possesses the characteristics of high strength, hardness [14–16], which make it advantageous as compared to other oxides. The incorporation of ductile ZrO_2 in the cermets represents a functional approach to toughen them [17,18]. As the material is subjected to external tensile stress, the compressive stress of the matrix on ZrO_2 is relaxed, and the crystal structure of ZrO_2 changes from tetragonal to monoclinic. This phase transition absorbs energy, relaxes the stress field at the crack tip and increases the crack growth resistance, thus, significantly improving the toughness of cermets. Mohammed A. Taha and Mahmoud F. Zawrah reported the achievement

* Corresponding author: mse_liwh@snut.edu.cn

of Al_2O_3-ZrO_2-Ni composites with improved properties. In this study, the Ni particles uniformly dispersed in the Al_2O_3-ZrO_2 matrix and the crystallite particle sizes increased with increasing the Ni content, whereas both dislocation density and lattice strain decreased [19]. Waheed S. AbuShanab and Rasha A. Youness studied the synthesis and structural properties characterization of TiO_2/ZrO_2/$CaSiO_3$ nanocomposites with a high-energy ball mill [20]. Medhat Ibrahim prepared zirconia-carbonated hydroxyapatite (ZrO2-CHA) nanocomposites using high-energy ball milling, and discovered that it will produce calcium zirconate ($CaZrO_3$) along with CHA and ZrO_2 [21].

The previous literature studies have mainly focused on the preparation and effect of the different alloying elements on the properties of Mo_2NiB_2-based cermets. K. Takagi reported on a family of Mo_2FeB_2 cermets fabricated by means of liquid phase sintering and expounded a boronizing sintering mechanism [22]. Further, Y. Yamasaki and K. Takagi explored the effect of Cr and V on the properties of Mo_2NiB_2 ternary boride [5,7,23]. In another study, L. M. Kubalova *et al.* revealed that powder compaction during the decomposition of the supersaturated Ni(Nb,B) and Ni(Mo,B) solid solutions led to the formation of cubic boride phases ($Ni_{21}Nb_2B_6$ and $Ni_{21}Mo_2B_6$) [24]. However, the effect of the second-phase particles (ZrO_2) on the properties of the Mo_2NiB_2-based cermets has not been systematically studied.

Recently, there has been considerable interest in using Mo_2NiB_2-based cermets in many top-end fields including wear resistance, corrosion resistance and heat resistance because of their superior properties such as mechanical and thermal properties [4,5]. Such applications are injection molding machine parts, hydrogen pumps, hot copper extruding dies, bearings for sea water pumps, cutters for heat sealers, drills for sand molds, etc. [4]. However, the problem reflected in the process of use is poor sintering activity and large brittleness, which greatly limit their application [3,7,23]. The purpose of the present study was to investigate the microstructure and fracture structure of the Mo_2NiB_2-based cermets, toughened with a ductile phase (ZrO_2). Mechanical alloying and vacuum sintering technology were used to prepare the Mo_2NiB_2-based cermets doped with different mass fractions (0.3 wt%, 0.6 wt% and 0.9 wt%) of ZrO_2. Subsequently, the fracture characteristics, especially the size and distribution of the second-phase particles (ZrO_2), of the developed Mo_2NiB_2-based cermets were investigated. Exploring the microstructure after deformation provided further insights into the strengthening effect of the second-phase particles. In addition, the influence of ZrO_2 addition on the mechanical properties of cermets was also analyzed.

II. Experimental Procedures

(1) Specimen preparation

Mo_2NiB_2 cermets with the nominal composition of x ZrO_2-Ni-6B-48Mo (in wt%, x = 0, 1.0, 1.5 and 2.0) were prepared based on the boronizing sintering reaction, named MNB, 1.0 ZrO_2-MNB, 1.5 ZrO_2-MNB and 2.0 ZrO_2-MNB, respectively. The commercially available Mo (99.95 wt%), B (99.99 wt%), Ni (99.99 wt%) and ZrO_2 (Y-PSZ, 99.95 wt%) powders were used as the raw powders, and their characteristics are listed in Table 1.

First, the accurately weighed amounts of the elemental powders of Mo, Ni, B and ZrO_2 were mixed under a protective atmosphere (argon) in a planetary ball mill (QM-3SP2). The ball milling was conducted at a speed of 150 rpm for 6 h, with a powder-to-ball weight ratio of 1:1, thereby yielding physically homogeneous powder particles. Prior to the boronizing sintering reaction, the powder mixture was pressed to form biscuits of the size Φ 30 mm. Afterwards, the biscuits were dried in a vacuum drying oven at 150 °C. Subsequently, these were placed on the alumina ceramic plate and sintered in a vacuum sintering furnace. The sintering temperature was maintained at 1 220 °C for 0.5 h followed by furnace cooling, and the vacuum was controlled below 1.0×10^{-2} Pa, thus, yielding the final sintered billets.

(2) Characterization

Phase identification was carried out using an XRD-7000s diffractometer. The microstructure of the specimens was characterized by means of transmission electron microscopy (TEM) (FEI F 20). Electron backscattered diffraction (EBSD) in SEM (FEI Quanta 650) was also carried out to obtain more detailed microstructural information. The TEM samples were prepared by means of a standard electro-polishing technique, using a twin-jet electro-polisher. The selected area electron diffraction (SAED) in TEM was employed to characterize the composition and structure of the grains and particles.

Table 1: The composition of the Mo_2NiB_2-based cermets as a function of the ZrO_2 fraction (wt%)

Label	Mo	Ni	B	ZrO_2 (Y-PSZ)
MNB	48.00	46.00	6.00	0
1.0 ZrO_2-MNB	47.52	45.54	5.94	1.0
1.5 ZrO_2-MNB	47.28	45.31	5.91	1.5
2.0 ZrO_2-MNB	47.04	45.08	5.88	2.0

The flexural strength and fracture toughness of the samples were determined in three-point bending tests. The flexural specimens with a cross-section of 3 × 4 mm^2 and a length of 26 mm as well as the fracture specimens with dimensions of 3 × 4 × 26 mm^3 and a notch of 2 mm cross-section were electro-discharge-machined and ground. The samples were subsequently tested in a universal testing machine (Instron 1185) by using a three-point bend fixture with a 20 mm span in ambient conditions. The crosshead speed was 0.5 mm/min during the flexural analysis, whereas it was 0.05 mm/min for evaluating the fracture toughness. In this study, prior to testing, the samples were electro-discharge-machined, ground and subsequently polished. Further, the experimental results represent an average value of at least five measurements.

III. Results

(1) Phase composition and microstructural characterization

Fig. 1 presents the XRD patterns of the Mo_2NiB_2-based cermets as a function of the of ZrO_2 content, after sintering at 1 220 °C. The sintered Mo_2NiB_2-based cermets exhibit diffraction peaks corresponding to Ni and Mo_2NiB_2. No other phases are observed, thus, indicating that the phase composition is not affected by the ZrO_2 content, which is consistent with the isothermal two-phase section of the Ni-rich portion of the Mo-Ni-B phase diagram [25, 26]. Moreover, the intensity of the diffraction peaks corresponding to the Mo_2NiB_2 phase is observed to be higher than the Ni phase.

Before sintering, the powder was mixed in a planetary ball mill. However, because the powder was mixed under argon protection, all the powders were not oxidized during the experiment. Therefore, the corresponding characteristic peaks of Mo, Ni, and B oxides were absent in the diffraction peaks. In addition, there were no diffraction peaks of zirconia in the XRD patterns, owing to the small amount of zirconia added, and the diffuse distribution in the samples [11].

The SEM image and EBSD maps in Fig. 2 further confirm the formation of two phases in the microstructure of the as-sintered Mo_2NiB_2-based cermets doped with 1.5 wt% ZrO_2. The Ni grains appear as the brightest phase, whereas the Mo_2NiB_2 grains demonstrate a dark contrast (Fig. 2(a)). Further, fine precipitates (dark) rich in Zr and O are observed to be distributed throughout the microstructure. The composition of these three phases was confirmed by the EDS analysis. So far, no literature study has reported the solubility of ZrO_2 in the Ni and Mo_2NiB_2 phases. As also observed from Fig. 2(a), the two phases reveal a fine grain structure formation. The formation of such a fine-grain microstructure represents a key feature of the materials produced by using the boronizing sintering technology. Fig. 2(b) reveals a few precipitated ZrO_2 particles in the Ni-based bonding phase, however, the formation of these precipitates indicates a low solubility limit in the Mo_2NiB_2 phase as well. Mo_2NiB_2 represents the ceramic phase with an area fraction of 57.5 %, in which the Ni (40.9 %) and ZrO_2 (1.6 %) phases are distributed uniformly. Fig. 2(c) shows the orientation distribution of the Ni and Mo_2NiB_2 grains along the different crystallographic directions indicated by the inverse pole images presented in the inset. The EBSD inverse pole figure map also reveals that the cermet consists of the equiaxed grains with an average grain size of 5 μm (Fig. 2(c)). Fig. 3 shows the size distribution of the Ni and Mo_2NiB_2 grains calculated using the EBSD measurements. As observed, a major fraction of grains has the size ranging from 0.1 to 20 μm. A larger variation in the grain size is observed for the Ni grains, whereas the Mo_2NiB_2 grains exhibit a narrow grain size distribution from 0.1 to 13 μm.

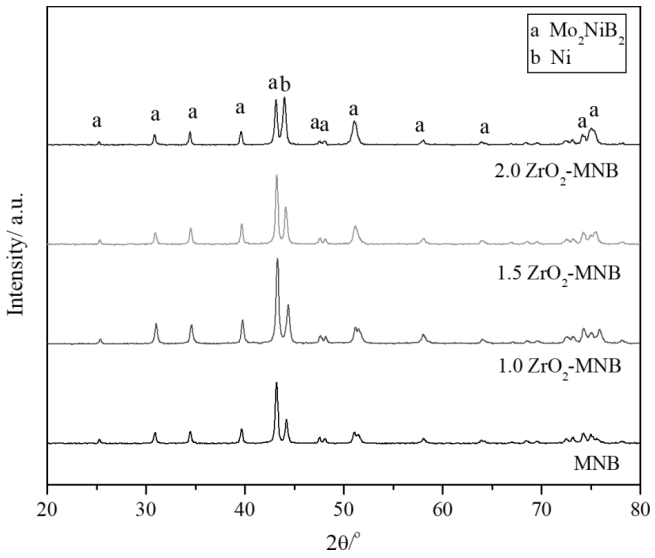

Fig. 1: XRD analysis of the Mo_2NiB_2-based cermets doped with different ZrO_2 amounts.

HRTEM analysis was performed to investigate the interface orientation relationship between the Mo_2NiB_2 phase and Ni grains (Fig. 4). Fig. 4(b) displays the HRTEM image of the two neighboring phases, exhibiting a ~3 nm interphase film in between. The two phases are noted to have different crystal structures and orientation relationship (Fig. 4(c) and 4(d)). The Ni phase corresponds to the FCC-structured lattice (a = ~0.352 nm). On the other hand, the Mo_2NiB_2 phase pertains to the orthorhombic crystal system (Immm space group), with lattice constants a = 0.455 nm, b = 0.707 nm and c = 0.318 nm [25, 27].

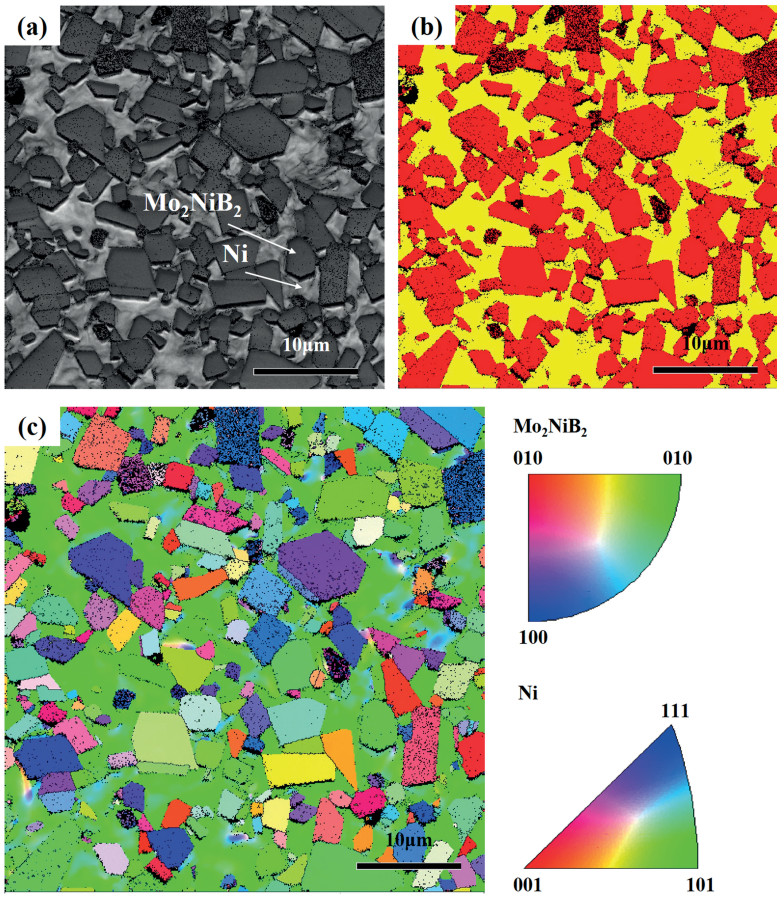

Fig. 2: The microstructure of the Mo_2NiB_2-based cermets doped with 1.5 wt% ZrO_2: (a) SEM image; (b) EBSD map; and (c) EBSD inverse pole figure map.

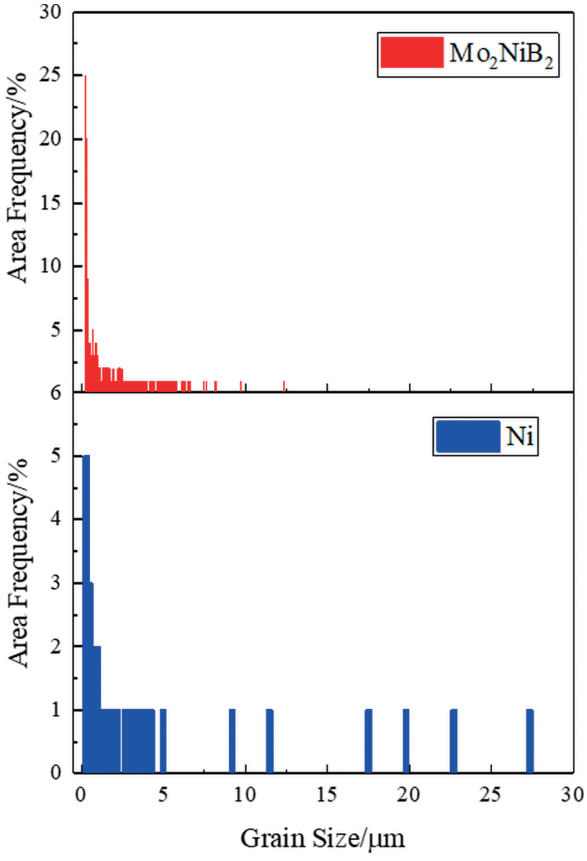

Fig. 3: The grain size distribution of the Mo_2NiB_2 and Ni phases.

(2) Flexural strength and fracture toughness

Fig. 5 shows the flexural engineering stress-strain curves of the Mo_2NiB_2-based cermets. The curve of the haploid cermet exhibits a near-linear-elastic region before fracture (3.01 % strain), with a small plastic strain on the MNB specimen. The curves of the Mo_2NiB_2-based cermets doped with 1.0 wt% ZrO_2 exhibit the linear-elastic region before ~ 3.05 % strain, with the maximum flexural strength under the action of an applied force before fracture. However, when the ZrO_2 content was increased to 1.5 wt% and 2.0 wt%, the strain of the sample decreases to 2.60 % and 1.83 %, respectively.

Fig. 6 exhibits the variation of the flexural strength and fracture toughness of the four cermet groups. The scatter plot diagram indicates that the flexural strength and fracture toughness exhibit an initial increase for the cermets MNB to 1.0 ZrO_2-MNB (with the ZrO_2 content increasing from 0 to 1.0 wt%). The flexural strength of 1.0 ZrO_2-MNB is determined to be 1397.33 MPa, which is 297.4 % higher than that of the 10 wt%-Cr-containing Mo_2NiB_2 ternary borides [23] and 24.5 % higher than that of the Mo_2NiB_2-Ni cermet (Ni-6B-60.5Mo) [28]. For the cermet sintered at 1 200 °C, the flexural strength was just about 960 ± 180 MPa and the hardness was not good enough to be evaluated by means of HRA [29].

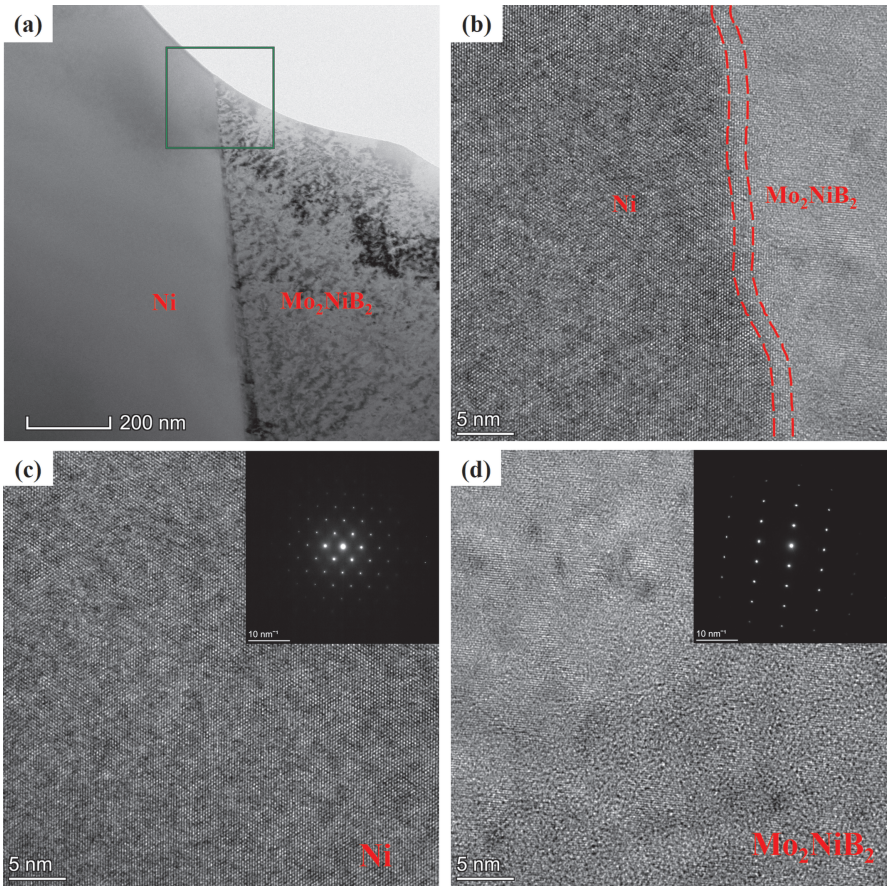

Fig. 4: (a) and (b) HRTEM images of the two neighboring Mo_2NiB_2 and Ni grains; and (c) and (d) high-resolution and diffraction spots for Mo_2NiB_2 and Ni grains.

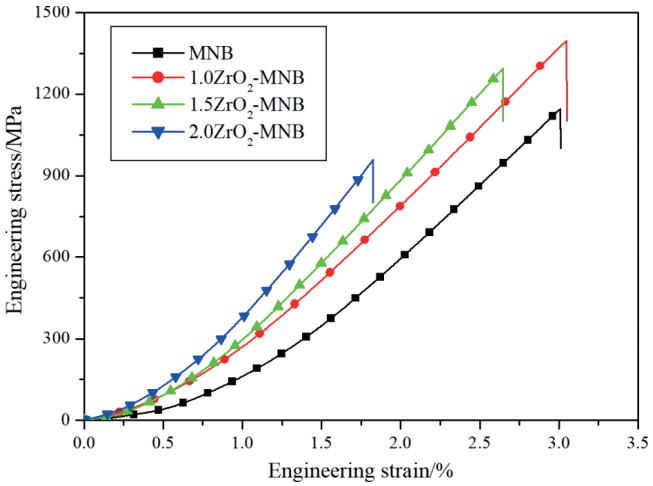

Fig. 5: The flexural engineering stress-strain curves of the Mo_2NiB_2-based cermets doped with different ZrO_2 amounts.

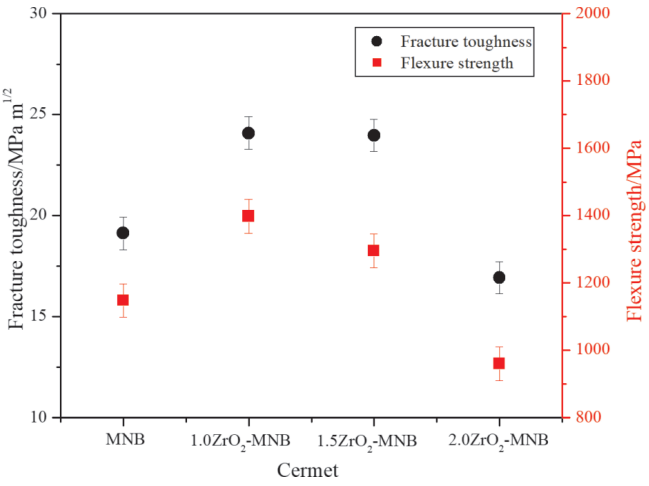

Fig. 6: The effect of the ZrO_2 content on the flexural strength and fracture toughness of the Mo_2NiB_2-based cermets.

The fracture toughness of 1.0 ZrO_2-MNB is determined to be 24.08 MPa $m^{1/2}$, which is 114.6 % and 105.61 % higher than the Mo_2NiB_2-Ni cermets, with the atomic ratio of Ni and B varying as 0.9 and 1.0, respectively [30]. The fracture toughness is comparable to that of Ni-5B-53.3Mo-xMn mass% cermets that were made by Ken-ichi Takagi [4]. The results given in [31] indicate that the highest fracture toughness corresponds to the state with Mo/(B + C) = 1, which is about 17.5 MPa $m^{1/2}$.

Thus, it is obvious that the Mo_2NiB_2-based cermets reveal synergistic enhancement and toughening owing to the addition of ZrO_2 particles. However, the flexural strength and fracture toughness of the developed cermets is observed to decrease gradually with increasing ZrO_2 content. As the doping amount of ZrO_2 exceeds 2.0 wt%, the strength and toughness of the Mo_2NiB_2-based cermets are noted to be significantly reduced.

Fig. 7 shows the SEM images of the fractured surfaces of the cermets after bending test. The dominant fracture

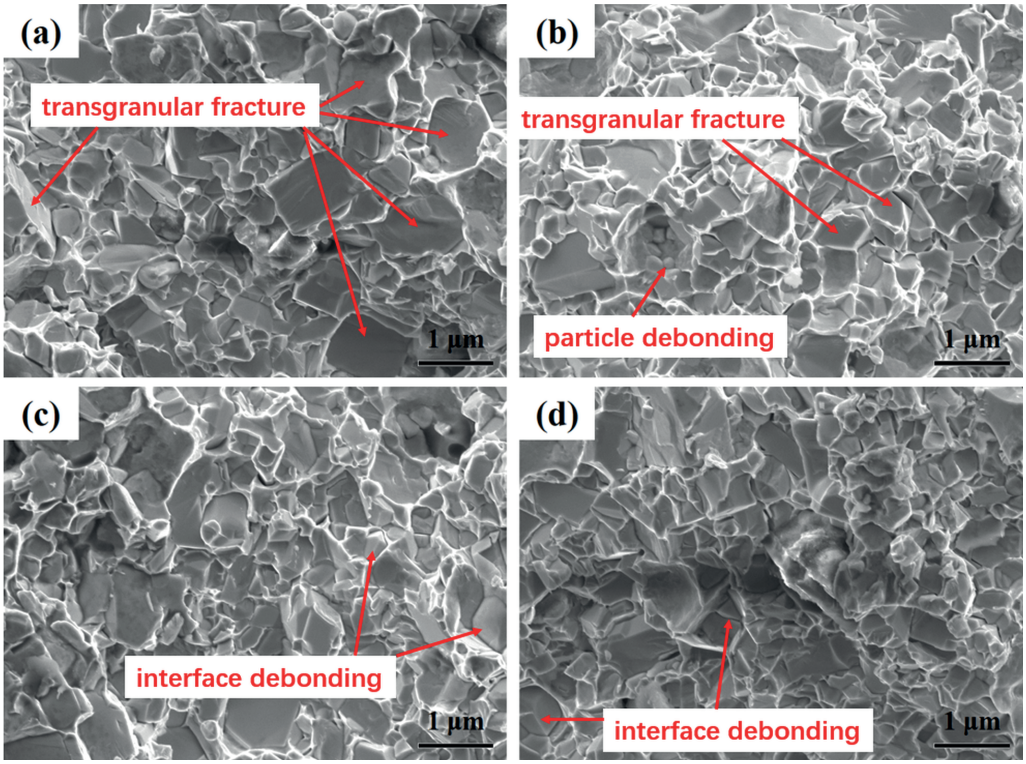

Fig. 7: The SEM images of the fractured surface after bending test. (a) MNB, (b) 1.0 ZrO_2-MNB, (c) 1.5 ZrO_2-MNB and (d) 2.0 ZrO_2-MNB.

mode for the cermets is the transgranular cleavage consisting of the quasi-cleavages, less inter-granular fracture, more tearing ridges and more dimples, where the fracture facets do not appear as the defined planes [32, 33].

In Fig. 7(a), there are multiple large coarse-particle phases (Mo_2NiB_2), and the fracture surface morphology of MNB cermet shows that the dominant failure mechanism exhibits transgranular fracture. According to the Hall-Petch formula, the yield strength will increase with a decrease of the crystalline grain size, so flexural strength and hardness are improved [34]. The highest flexural strength and fracture toughness are obtained with the ZrO_2 content of 1.0. The excellent flexural strength and fracture toughness are attributed to relative fine grains and homogeneous two-phase microstructure (Ni and Mo_2NiB_2), as shown in Fig. 7(b), in which neither coarsening of Mo_2NiB_2 grains nor large quantity of a third phase occurs. An increasing ZrO_2 addition promoted grain refinement, which changed the fracture mode from transgranular fracture to interface debonding (Fig. 7(c) and (d)), and accordingly decreased the fracture toughness of the Mo_2NiB_2-based cermets.

Fig. 8 shows the typical dislocation microstructure of the 1.0 ZrO_2-MNB specimen deformed to 1.5 % strain in the bending test. The TEM observation confirms a high density of the closely spaced dislocations within the Ni grains, with a fraction of these present in the tangles and networks (Fig. 8 (a) and (b)). Mo_2NiB_2 grains growing in different directions interlock with each other to prevent crystal boundary slip, thereby enhancing the mechanical strength (Fig. 8 (c) and (d)). Moreover, the fine-grained microstructure not only strengthened but also toughened the MNB cermets.

IV. Strengthening Mechanism

The significant improvements in the mechanical properties of the MNB cermets doped with ZrO_2 indicate that the combination of ZrO_2 and MNB synergistically contributes to the strength and toughness. Further, significant pinning crystal boundaries and slip surfaces are observed in the TEM images of the Mo_2NiB_2 phase in the cermet specimens, as shown in Fig. 8.

Owing to the difficulty in collating the different strengthening mechanisms in a single constitutive equation, a simple proportional weight method based on the intrinsic strength of pure Ni (σ_0) and Mo_2NiB_2 (σ_1) and second phase (ZrO_2) particle (σ_2) grain boundaries (σ_{NZ}, σ_{MZ} and σ_{NM}) has been considered for the prediction of the total strength (σ_y) as follows:

$$\sigma_y = \sigma_0 + \sigma_1 + \sigma_2 + \sigma_{NZ} + \sigma_{MZ} + \sigma_{NM} \quad (1)$$

The contribution of the Ni grains, Mo_2NiB_2 grains and grain boundaries (σ_{NM}) to the strength is constant. Besides, the ZrO_2 particles are mainly located in the Mo_2NiB_2 grains, thus, the σ_{NZ} value is negligible. Further, the impact of σ_0, σ_1, σ_{NZ} and σ_{NM} on the strength has not been considered.

The contribution of the ZrO_2 particle strengthening (σ_2) can be quantitatively evaluated by using the Orowan model. As the ZrO_2 particles are distributed in the Ni and Mo_2NiB_2 grains, the ZrO_2 particle strengthening term can be determined based on these ZrO_2 particles. Owing to a small content of ZrO_2 in the Ni grains, the influence of the ZrO_2 particle strengthening on these grains can be neglected. Thus, an estimated Orowan strengthening can be evaluated from the ZrO_2 particles using the equation:

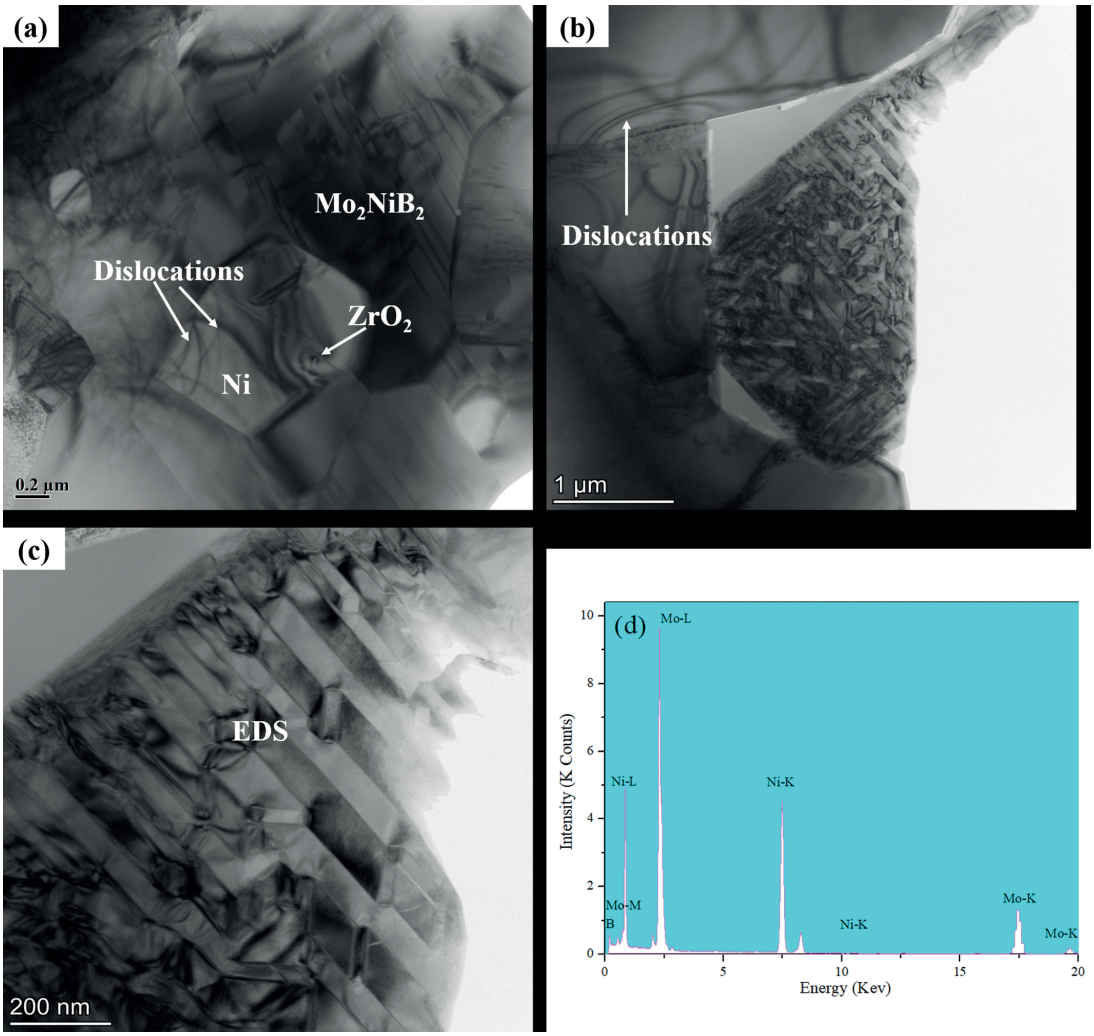

Fig. 8: The dislocation configuration of the 1.0 ZrO_2-MNB specimen after the bending test. (a) and (b) A high density of dislocations with tangles distributed in the Ni grains, (c) Mo_2NiB_2 grains growing in different directions interlocking with each other, and (d) depicts the responding EDS analyses in Fig. 8(c).

$$\sigma_2 = \frac{m\mu b}{1.18 \times 2\pi(\lambda - \Phi)} \ln\left(\frac{\Phi}{2b}\right) \quad (2)$$

where m, μ and b are the Taylor factor taken as 2.5, elastic modulus taken as 415 GPa [23] and Burgers vector used as 0.228 m, respectively. Additionally, λ is the spacing of the staggered shear planes, which can be estimated with TEM, and Φ is the size of the ZrO_2 particles.

The efficient load transfer, σ_{IS}, between the Mo_2NiB_2 grains and the hard ZrO_2 grains reinforcement occurs during compressive testing. Mostly, when the interfacial contact between Mo_2NiB_2 and ZrO_2 grains is good enough and it is represented as follows:

$$\sigma_{IS} = 0.5 V_f \sigma_{YM} \quad (3)$$

where V_f represents the volume fraction of ZrO_2 grains reinforcement and σ_{YM} represents the yield stress of ZrO_2-MNB cermet [35].

On the other hand, the differential interfacial wettability between the ZrO_2 and Mo_2NiB_2 grains reduces the strength of the cermets, thus, the rule of minus expression is employed in order to calculate the effective grain boundary strength as:

$$\sigma'_{IS} = K(\sigma_1 + \sigma_2)A_C \quad (4)$$

where *Ac* is the grain boundary area, which can be roughly replaced by the ZrO_2 particle surface area, and K is a coefficient related to the physical and chemical compatibility.

Therefore, as the slip is carried out during the deformation process, the dislocation will gradually occur around the ZrO_2 particles. Thus, the ZrO_2 particles hinder the grain boundary slip, thereby making the deformation of the cermet more difficult as well as enhancing the strength. However, an increase in the ZrO_2 content also makes them more likely to agglomerate, thus, reducing the grain boundary strength. The higher the ZrO_2 content is, the more obvious is the reduction in the grain boundary strength. Therefore, the total strength of the Mo_2NiB_2-based cermets doped with ZrO_2 particles results from the combination of two factors.

$$\sigma_{NM} = \sigma_{IS} + \sigma'_{IS} \quad (5)$$

After the indentation analysis of the MNB cermets, a number of cracks are observed at the edge of the indentation imprint, which have been used to further investigate the fracture behavior of the cermets. For instance, a typical crack in the 1.0 ZrO_2-MNB cermet in Fig. 9 illustrates

the crack propagation path and fracture morphology. The crack deflection (white rectangular dotted line in Fig. 9 (a)), crack bridging (black arrow in Fig. 9 (a)), transgranular cracks (white arrow in Fig. 9 (a)) and pulled out ZrO_2 particles are observed, and the agglomerated ZrO_2 particles (white arrow in Fig. 9 (b)) are subsequently formed, as clearly observed in the case of the 1.0 ZrO_2-MNB cermet. The crack deflection and transgranular cracks consume more energy than the original path, and the crack bridging phenomenon inhibits crack growth. These toughening mechanisms lead to energy dissipation during the crack propagation, thus, leading to enhanced fracture toughness [36].

Fig. 9: The crack propagation path and fracture morphology in the case of the 1.0 ZrO_2-MNB cermet.

In addition, a part of the crack propagation energy is consumed by ZrO_2 as the cermets break (the specific process is shown in Fig. 9 (b)), which improves the fracture toughness of the MNB cermets doped with ZrO_2 particles. As the cracks grow to the ZrO_2 particles, the induced tensile stress transforms the ZrO_2 phase from tetragonal to monocline at the crack tip [37,38]. Moreover, a certain volume expansion and shear strain are produced, thus, leading to the compressive stress and further consuming the tensile stress of the crack propagation. Thus, the crack tip energy is absorbed, and the crack propagation stops. The fracture mode of the Z-MNB cermets is observed to be crack deflection, crack bridging, transgranular cracks and crack propagation hindered owing to the ZrO_2 phase transformation.

For the Mo_2NiB_2-based cermets doped with ZrO_2 particles, increasing the ZrO_2 content at the crack tip consumes a large fraction of the plastic deformation work, thus, enhancing the fracture toughness [24]. However, this approach leads to a reduction in the strength of the cermets. Assuming that the size and volume fraction of the Mo_2NiB_2 and Ni phases to be the same, the designed and experimentally validated optimal ZrO_2 content for the Mo_2NiB_2 based cermets is 1.0 wt%, which exhibits the highest fracture toughness of 24.08 MPa $m^{1/2}$.

V. Conclusions

In summary, the Mo_2NiB_2-based cermets with the nominal composition of x ZrO_2-Ni-6B-48Mo (in wt%, x = 0, 1.0, 1.5 and 2.0) were successfully prepared by means of the boronizing sintering process. Subsequently, the microstructure and mechanical properties as well as the strengthening and toughening mechanisms of the developed materials were studied. The main conclusions are presented as follows:

(1) The microstructure of the sintered cermets exhibits that the Mo_2NiB_2 particles are distributed in the continuous Ni matrix. A few spherical or ellipsoidal ZrO_2 particles at the nano- and submicron scales are located at the grain boundaries and within the Mo_2NiB_2 grains.

(2) 1.0 ZrO_2-MNB cermet is observed to exhibit optimal mechanical properties. Its flexural strength and fracture toughness are determined to be 1 397.33 MPa and 24.08 MPa.$m^{1/2}$, respectively. Overall, the flexural strength and fracture toughness of the ZrO_2 ceramics are noted to increase by 25.94 % and 21.78 %, respectively, as compared with the MNB cermet.

(3) The strength enhancement results due to the improved dislocation density as well as the grain boundary slip obstruction caused by the interlocked Mo_2NiB_2 grains. Further, the improved toughness can be attributed to the crack deflection, crack bridging, transgranular cracks and ZrO_2 phase transformation.

Acknowledgements

This work was financially supported by the National Natural Science Foundation of China under Project No. 51602186, the Shaanxi Province Natural Science Foundation of China under Project No. 2020JM-599, 2020JQ-870 and the Opening Fund of National and Local Joint Engineering Laboratory for Slag Comprehensive Utilization and Environmental Technology under Project No. SLGPT2019KF01 – 04.

The authors would like to express their gratitude to EditSprings (https://www.editsprings.com/) for the expert linguistic services provided.

References

1 Hirata, K., Iwanaga, K., Yamasaki, Y., Takagi, K.: Development of Mo_2NiB_2 base cermets with high strength and excellent corrosion resistance for plastic injection molding machine parts, *J. Jpn. Soc. Powder Powder Metall.*, **53**, 447 – 451, (2006).

2 Dent, A.H., Horlock, A.J., McCartney, D.G., Harris, S.: Microstructure formation in high velocity oxy-fuel thermally sprayed Ni-Cr-Mo-B alloys, *Mater. Sci. Eng. A*, **283**, 242 – 250, (2000).

3 Takagi, K.: High tough boride base cermets produced by reaction sintering, *Mater. Chem. Phys.*, **67**, 214 – 219, (2001).

4 Takagi, K.: Development and application of high strength ternary boride base cermets, *J. Solid State Chem.*, **179**, 2809 – 2818, (2006).

5 Yamasaki, Y., Nishi, M., Takagi, K.: Development of very high strength Mo_2NiB_2 complex boride base hard alloy, *J. Solid State Chem.,* **177**, 551 – 555, (2004).

6 Takagi, K., Yamasaki, Y., Komai, M.: High-strength boride base hard materials, *J. Solid State Chem.*, **133**, 243 – 248, (1997).

7 Takagi, K., Yamasaki, Y.: Effects of Mo/B atomic ratio on the mechanical properties and structure of Mo_2NiB_2 boride base cermets with Cr and V additions, *J. Solid State Chem.*, **154**, 263 – 268, (2000).

8 Chang, S., Hung, L., Yang, T.: The effects of adding micro-scaled niobium carbide on the microstructure, mechanical strength and polarization resistance of the Ti-8Mo-4Co-xNbC composites, *Mater. Chem. Phys.*, **235**, 121743, (2019).

9 He, L., Gao, Y., Li, Y., Liu, Z., Yuan, W., Chen, W., Zhao, S., Liu, H., Yan, W.: Effect of TiB_2/WC addition on the oxidation behavior of Ti(C,N)-304ss cermets during the early oxidation stage, *Corros. Sci.*, **159**, 108 – 118, (2019).

10 Lin, N., Zhao, L., Ma, C., Wang, Z., Wen, J., He, Y.: Enhanced mechanical properties and high temperature oxidation resistance of Ti(C,N)-based cermets containing Zr, *J. Alloy Compd.*, **788**, 649 – 657, (2019).

11 Li, R., Li, B., Wang, T., Ren, S., Chen, X., Wang, J., Zhang, G.: Improved fracture toughness of a Mo-12Si-8.5B-3Zr alloy by grain coarsening and its multiple toughening mechanisms, *J. Alloy Compd*., **743**, 716 – 727, (2018).

12 Wang, J., Li, B., Li, R. *et al.*: High toughness and strength of Mo-12Si-8.5B-ZrB2 alloy resulting from a bimodal α-mo grain structure, *Inter. J. Refract. Met. Hard Mater.*, **86**, 105 – 129, (2020).

13 Hochmuth, C. Schliephake, D., Völkl, R. *et al*.: Influence of zirconium content on microstructure and creep properties of Mo-9Si-8B alloys, *Intermetallics*, **48**, 3 – 9, (2014).

14 Du, W., Ai, Y., He W., Chen, W. Liang, B., Lv, C.: Formation and control of "intragranular" ZrO_2 strengthened and toughened Al_2O_3 ceramics, *Ceram. Int.*, **46**, 8452 – 8461, (2020).

15 Rahmani, K., Majzoobi, G.H., Sadooghi, A., Kashfi, M.: Mechanical and physical characterization of Mg-TiO_2 and Mg-ZrO_2 nanocomposites produced by hot-pressing, *Mater. Chem. Phys.*, **246**, 122844, (2020).

16 Oke, S.R., Falodun, O.E., Okoro, A.M., Tshephe, T.S., Olubambi, P.A.: Effect of ZrO_2 addition on densification and properties of spark plasma sintered Ti_6Al_4V-ni, *Mater. Today*, **18**, 2454 – 2460, (2019).

17 Wang, B., Wang, N., Yang, Y., Zhong, H., Ma, M., Zhang, X., Liu, R.: Fabrication, microstructures and mechanical properties of ZrO_2 dispersion-strengthened Q345 steel, *T. Nonferr Metal Soc.*, **28**,1132 – 1140 (2018).

18 Ajay Kumar, V., Rama Murty Raju, P., Ramanaiah, N., Siriyala, R.: Effect of ZrO_2 content on the mechanical properties and microstructure of HAp/ZrO_2 nanocomposites, *Ceram. Int.*, **44**, 10345 – 10351, (2018).

19 Taha, M.A., Zawrah, M.F.: Fabrication of Al_2O_3-ZrO_2-Ni composites with improved toughness using nano powders prepared by mechanical alloying, *Ceram. Int.*, **46**, 19519 – 19529, (2020).

20 AbuShanab, W.S., Moustafa, E.B., Taha, M.A., Youness, R.A.: Synthesis and structural properties characterization of titania/zirconia/calcium silicate nanocomposites for biomedical applications, *Appl. Phys. A*, **126**, 787, (2020).

21 Youness, R.A., Taha, M.A., Ibrahim, M.A.: *In vitro* bioactivity, molecular structure and mechanical properties of zirconia-carbonated hydroxyapatite nanobiocomposites sintered at different temperatures, *Mater. Chem. Phys.*, **239**, 122011, (2020).

22 Takagi, K., Ozaki, S., Komai, M., Matsuo, S.: Sintering mechanism and physical properties of Mo_2FeB_2 type complex boride, *Trans. Mat. Res. Soc. Jpn*., 14A, 475 – 478, (1994)

23 Takagi, K., Koike, W., Momozawa, A., Fujima, T.: Effects of cr on the properties of Mo_2NiB_2 ternary boride, *Solid State Sci.*, **14**, 1643 – 1647, (2012).

24 Kubalova, L.M., Fadeeva, V.I.: The effect of deformation treatment on the decomposition of supersaturated Ni(Nb,B) and Ni(Mo,B) solid solutions synthesized by mechanical alloying, *J. Alloy. Compd.*, **586**, S61 – S64, (2014).

25 Kubliy, V.Z., Bondar, A.A., Utkin, S.V., Petyukh, V.M., Lysenko, S.I., Velikanova, T. Ya.: Phase equilibria in the nickel corner of the mo-ni-B system at temperatures close to melting, *Powder Metall. Met. C*+, **47**, 211 – 222, (2008).

26 Utkina, S.V., Kubliia, V.Z., Sleptsova, S.V., Bondara, A.A., Levchenkoa, P.P., Osokina, G.A., Velikanova, T.Ya.: Solidus surface of the Mo-Ni-B system, *J. Superhard Mater.*, **41**, 3 – 19, (2019).

27 Utkin, S.V., Kublii, V.Z., Sleptsov, S.V., Bondar, A.A., Levchenko, P.P., Osokin, G.A., Velikanov, T.Ya.: Solidus surface of the Mo-Ni-B system, *J. Superhard Mater.*, **41**, 287 – 301, (2019).

28 Zhang, L., Huang, Z., Liu, Y., Shen, Y., Li, K., Cao, Z., Ren, Z., Jian, Y.: Effects of mechanical ball milling time on the microstructure and mechanical properties of Mo_2NiB_2-ni cermets, *Materials*, **12**, 1926, (2019).

29 Yuan, B., Zhang, G.J., Kan, Y.M., Wang, P.L.: Reactive synthesis and mechanical properties of Mo_2NiB_2 based hard alloy, *Inter. J. Refract. Met. Hard Mater.*, **28**; 291 – 296, (2010).

30 Zhang, L., Huang, Z., Liu, Y., Shen, Y., Li, K., Cao, Z., Ren, Z., Jian, Y.: Effect of ni content on the microstructure, mechanical properties and erosive wear of Mo_2NiB_2-Ni cermets, *Ceram. Int.*, **45**, 19695 – 19703, (2019).

31 Vershinina, T.N., Ivanov, M.B., Rimsha, P.B.: The effect of carbon on phase composition and microstructure of cermets based on Mo_2NiB_2 boride, *Inter. J. Refract. Met. Hard Mater.*, **100**, 105650, (2021).

32 Yu, H., Zheng, Y., Liu, W., Zheng, J., Xiong, W.: Effect of mn content on the microstructure and mechanical properties of Mo_2FeB_2 based cermets, *Inter. J. Refract. Met. Hard Mater.*, **28**, 286 – 290, (2010).

33 Yu, H., Liu, W., Zheng, Y.: Effect of carbon content on the microstructure and mechanical properties of Mo_2FeB_2 based cermets, *Inter. J. Refract. Met. Hard Mater.*, **29**, 724 – 728, (2011).

34 Yu, H.Z., Zheng, Y., Liu, W.J., Pang, X.M., Zheng, J.Z., Xiong, W.H.: Effect of Mo/B atomic ratio on the microstructure and mechanical properties of Mo_2FeB_2 based cermets, *Inter. J. Refract. Met. Hard Mater.*, **28**, 338 – 342, (2010).

35 AbuShanab, W.S., Moustafa, E.B., Ghandourah, E., Taha, M.A.: Effect of graphene nanoparticles on the physical and mechanical properties of the Al2024-graphene nanocomposites fabricated by powder metallurgy, *Results Phys.*, **19**, 103343, (2020).

36 Yu, H., Liu, W., Zheng, Y.: Microstructure and mechanical properties of liquid phase sintered Mo_2FeB_2 based cermets, *Mater. Des.*, **32**, 3521 – 3525, (2011).

37 Cui, C., Zhu, X., Liu, S., Li, Q., Zhang, M., Zhu, G., Wei, S.: Effect of nano-sized ZrO_2 on high temperature performance of Mo- ZrO_2 alloy, *J. Alloy Compd.*, **768**, 81 – 87, (2018).

38 Li, F., Zhang, X., Sui, C., Wu, J., Wei, H., Zhang, Y.: Microstructure and mechanical properties of Al_2O_3-ZrO_2 ceramic deposited by laser direct material deposition, *Ceram. Int.*, **44**, 18960 – 18968, (2018).